Journal of Magnetic Resonance **155,** 150–155 (2002)
doi:10.1006/jmre.2002.2508, available online at http://www.idealibrary.com on IDEAL®

COMMUNICATIONS

Signal Enhancement in the Triple-Quantum Magic-Angle Spinning NMR of Spins-$\frac{3}{2}$ in Solids: The FAM–RIACT–FAM Sequence

P. K. Madhu[1] and M. H. Levitt

Department of Chemistry, University of Southampton, Southampton SO17 1BJ, United Kingdom

Received October 30, 2001; revised December 26, 2001

We achieve a significant signal enhancement for the triple-quantum magic-angle spinning NMR of a spin-$\frac{3}{2}$ system, by using an amplitude-modulated radiofrequency field, followed by a selective 90° pulse and a phase-shifted strong rf field, for the triple-quantum excitation, and an amplitude-modulated radiofrequency field for the conversion of triple-quantum coherence to observable single-quantum coherence. The experiment is demonstrated on the ^{87}Rb NMR of polycrystalline rubidium nitrate.

The introduction of multiple-quantum magic-angle spinning (MQMAS) (*1, 2*) has made the high-resolution solid-state NMR of half-integer quadrupolar nuclei routinely feasible. The method has found applications in many fields including catalysts, zeolites, minerals, and glasses (*3–6*).

MQMAS was first implemented using a simple two pulse scheme (*2*), in which the first pulse is used for the excitation of multiple quantum coherence (MQC) and the second pulse for the conversion of MQC into observable single quantum coherence (1QC). Both of these steps are rather inefficient, so the application of this experiment was hampered by its low sensitivity.

Much effort has been expended in improving the sensitivity of MQMAS experiments. Until recently, most progress was made in improving the conversion efficiency of the MQC into 1QC. For example, a long unmodulated radiofrequency (rf) pulse lasting one quarter of a rotor period was used to implement rotor-induced adiabatic coherence transfer (RIACT) (*7*). Modulated rf field methods were also introduced, such as the fast amplitude modulation (FAM) (*8–10*) and double frequency sweep (DFS) (*11–13*) methods.

It has proven to be more difficult to enhance the efficiency of the excitation part of the experiment. The RIACT-II (*14*) scheme uses a long unmodulated rf pulse lasting one quarter of a rotor period for both the excitation and conversion parts of the pulse sequence. Unfortunately, the enhancement in signal strength by RIACT-II is often accompanied by distortions in the anisotropic lineshapes, and hence a loss of spectral information. Recently, RIACT excitation of MQC was combined with a FAM sequence for conversion into SQC, leading to appreciable signal enhancements while avoiding unacceptable anisotropic lineshape distortion for spin-$\frac{3}{2}$ systems (*15*). In the discussion below, this is called the RIACT-FAM method (*16*).

In a related development, a FAM sequence lasting one rotor period, followed by a selective 90° pulse, was used for the enhancement of central-transition single quantum signals in the MAS of half-integer quadrupolar nuclei (*17*). Experimentally, the enhanced signal was a factor of 1.8 larger than that obtained with a hard 90° pulse. The enhancement is due to the selective saturation of the satellite transitions by the FAM sequence which enhances the population difference across the central transition. This application of FAM is termed rotary-assisted population transfer (RAPT) (*17*). The limiting theoretical ratio of the enhanced to the non-enhanced signals is $I + \frac{1}{2}$, where I is the spin quantum number (*17*).

An initial FAM sequence has also been shown to enhance the spin-$\frac{3}{2}$ MQMAS signals obtained with the RIACT-II scheme (*18*). However, as remarked above, the RIACT-II scheme usually gives rise to distorted anisotropic line shapes, so the applications of this FAM-RIACT-II combination are expected to be limited.

In this communication, we show that the signal strengths produced by the RIACT-FAM method of Goldbourt *et al*. (*15*) may be enhanced by a factor of around 1.5 by preceding the pulse sequence with another FAM scheme in order to implement rotary-assisted population transfer. This FAM–RIACT–FAM method achieves high signal strengths in spin-$\frac{3}{2}$ systems without appreciable lineshape distortions. We report the pulse sequence used for the experiment, numerical simulations which substantiate the arguments and experimental results on the ^{87}Rb NMR of polycrystalline rubidium nitrate, $RbNO_3$.

All MQMAS experiments were performed on a Chemagnetics CMX-200 MHz spectrometer using a 4-mm double resonance probe at a magic-angle spinning frequency of 10.0 kHz. ^{87}Rb NMR signals were observed at a Larmor frequency of 65.502 MHz.

[1] To whom correspondence should be addressed. E-mail: madhu@soton.ac.uk.

1090-7807/02 $35.00

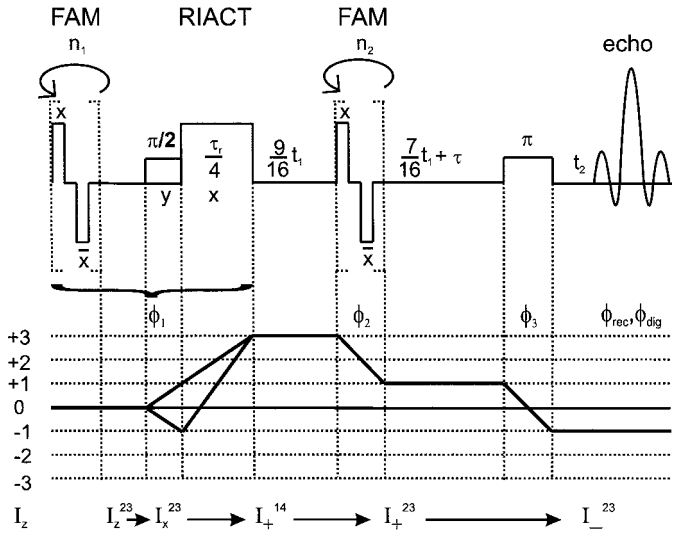

FIG. 1. Schematic of the FAM–RIACT–FAM sequence with the relevant spin operators that are chiefly active. The scheme makes use of the split-t_1 method followed by a τ delay and a selective 180° pulse to incorporate the whole-echo acquisition.

A fully packed rotor of polycrystalline $RbNO_3$ was used for the experiments. $RbNO_3$ has three ^{87}Rb sites, Rb(1) (1.7 MHz, 0.2), Rb(2) (2.0 MHz, 1.0) and Rb(3) (1.8 MHz, 0.5), where the numbers in brackets refer to the quadrupole coupling constant C_Q and asymmetry parameter η (*19*).

The pulse sequence for the FAM–RIACT–FAM method is shown in Fig. 1 together with the selected coherence transfer pathways. Each FAM loop consisted of the sequence $\beta_0 - \tau_w - \beta_\pi - \tau_w$, where β_ϕ represents a rf pulse of phase ϕ and duration τ_p corresponding to $\omega_{nut}\tau_p = \beta$, where $\omega_{nut} = |\gamma(I + \frac{1}{2})B_{rf}|$ is the central transition nutation frequency during the pulse. The pulse duration τ_p and window duration τ_w during the FAM loops were $\tau_p = \tau_w = 1$ μs. This corresponds to a nutation frequency of 250 kHz. An optimization of the FAM pulse lengths and interpulse delays is expected to enhance the signal intensity further. The rf nutation frequency during the FAM loops was $\omega_{nut}/2\pi = 70$ kHz. The number of repetitions of the two FAM loops were $n_1 = 25$ and $n_2 = 3$. The overall duration of the first FAM loop, used for implementing the RAPT enhancement, corresponds to one whole rotor period.

The pulse sequence in Fig. 1 involves selective $\pi/2$ and π pulses applied to the central transition. These pulses used a rf nutation frequency of 20 kHz. The long rf pulse used for the RIACT scheme employed a nutation frequency of 70 kHz and had a duration of 25 μs, corresponding to one quarter of a rotor period. The two-dimensional (2D) experiments employed a split-t_1 (*20*) whole-echo (*21*) method to obtain pure absorption spectra with separation of the isotropic signals in the ω_1 dimension. A total of 128 t_1 increments were acquired, each of which was obtained with 96 phase-cycled transients. The recycle delay was 1 s. The evolution interval t_1 was incremented in steps of 20 μs. The signal was digitized in t_2 using a sampling interval of 50 μs. The delay τ was set to the value $\tau = 5.120$ ms, so that the echo signal appeared in the middle of the acquisiton window. The rf phases were cycled according to $\phi_1 = \mathcal{M}\pi/6$, $\phi_2 = 0$, $\phi_3 = floor(\frac{\mathcal{M}}{12})\pi/4$, $\phi_{rec} = 0$ and $\phi_{dig} = -3\phi_1 + 2\phi_3$ in order to select the coherence pathways indicated in Fig. 1. Here $\mathcal{M} = 0, 1, 2, \ldots, 95$ is the transient counter, ϕ_{rec} is the rf receiver phase, and ϕ_{dig} is the postdigitization phase shift (*22*). An abbreviated phase cycle, which achieves the same degree of selectivity using 23 steps, will be described elsewhere (*23*).

In the following discussion, the performance of the FAM–RIACT–FAM is compared with a number of other MQMAS methods, including the original two-pulse scheme (CW-CW) (*2, 7, 24*), the RIACT-II method (*14*), the pulse-FAM method (CW-FAM) (*8*), the RIACT–FAM method (*15*), and the FAM–RIACT-II method (*18*). In these comparisons, all relevant pulse sequence parameters are the same as those used in the FAM–RIACT–FAM sequence. The MQ excitation pulses used in the two-pulse scheme (*2, 7, 24*) had a duration of 8 μs. The MQ $\rightarrow$ 1Q conversion pulse in the two-pulse scheme (*2, 7, 24*) had a duration of 2 μs.

In this discussion, we index the Zeeman eigenstates of a half-integer spin according to $|1\rangle = |+\frac{3}{2}\rangle$, $|2\rangle = |+\frac{1}{2}\rangle$, $|3\rangle = |-\frac{1}{2}\rangle$, $|4\rangle = |-\frac{3}{2}\rangle$. Single-transition operators may then be defined in the usual way (*25*). The performance of the FAM–RIACT–FAM sequence in a spin-$\frac{3}{2}$ system is based upon the following observations:

- The initial spin density operator is proportional to $I_z = 3I_z^{14} + I_z^{23}$; i.e., the largest population difference exists across the two extreme Zeeman eigenstates.
- As described in Ref. (*17*), the extended FAM sequence leads to an equalization of the populations of the outer state pairs $\{|1\rangle, |2\rangle\}$ and $\{|3\rangle, |4\rangle\}$, leading to a density operator roughly proportional to $2I_z^{14} + 2I_z^{23}$. The effect is to reduce the population difference across the extreme eigenstates by a factor of $\frac{2}{3}$ and to enhance the population difference across the central transition by a factor of two.
- The selective 90° pulse following the extended FAM sequence mainly converts the enhanced central transition population difference, I_z^{23}, to central transition coherence, I_x^{23}. This process is depicted (loosely) by the transformation $I_z^{23} \rightarrow I_x^{23}$ in Fig. 1.
- The strong rf irradiation for an interval of $\frac{1}{4}\tau_r$ leads to a reasonably efficient conversion of central transition 1QC (I_x^{23}) to three-quantum coherence (3QC), through rotor-assisted adiabatic coherence transfer, RIACT (*7, 14*). Note that both components $|2\rangle\langle 3|$ and $|3\rangle\langle 2|$ contribute to the (+3)-quantum coherence $|1\rangle\langle 4|$, as indicated by the two coherence transfer pathways in Fig. 1.
- After the first part of the split evolution interval, the (+3)-quantum coherence $I_+^{14} = |1\rangle\langle 4|$ is converted by the second FAM sequence into (+1)-quantum coherence $I_+^{23} = |2\rangle\langle 3|$, as described in Refs. (*9, 21*). Note that this process is not

symmetric, in the sense that the transfer of I_+^{14} into the (-1)-quantum coherence $I_-^{23} = |3\rangle\langle 2|$ is weak. As discussed in Refs. (*9, 21*), this lack of symmetry is favourable, since the symmetrical pathway $(+3) \rightarrow (-1)$ does not lead to an echo of the second-order quadrupolar interaction, and is of no use in MQMAS NMR. If a RIACT sequence is used for the $(+3) \rightarrow (+1)$ conversion on the other hand, the superfluous $(+3) \rightarrow (-1)$ pathway is enhanced at the expense of the desirable $(+3) \rightarrow (+1)$ pathway, which leads to a loss of echo intensity.

• The selective central transition π pulse leads to an echo of the (-1)-quantum signals, allowing the acquisition of pure absorptive 2D spectrum, as recommended by Massiot *et al.* (*19, 21*).

Figure 2 shows a set of 3Q echo simulations for different pulse sequences. The simulations are done for a powder sample containing a spin-$\frac{3}{2}$ site with quadrupole parameters $C_Q = 2.0$ MHz and $\eta = 1.0$, corresponding to the Rb(1) site in $RbNO_3$. The signal during t_2 is shown for a 3Q evolution time of $t_1 = 900$ μs. The second-order quadrupolar echo is observed at $t_2 = 700$ μs. The magnetic field was assumed to be 4.7 T.

All simulations were performed using the program SIMPSON (*26*). A total of 615 quadrupolar orientations, selected according to the ZCW scheme (*27–29*), were used to simulate the powder response. The simulation parameters were the same as used for the experiments, outlined in Section 2.

Figures 2a and 2b show 3Q echo signals obtained with the original two-pulse sequence (*2, 7, 24*) and the RIACT-II method (*14*) respectively. Figure 2c shows the enhancement in the RIACT-II signal intensity by the application of an initial FAM modulation leading to rotor assisted population transfer (*18*). The simulated signals are also enhanced by using FAM for the $(+3) \rightarrow (+1)$ conversion, as shown in Figs. 2d and 2e. Figure 2f shows that the FAM–RIACT–FAM scheme produces a further increase in the simulated echo intensity.

The quadrupolar parameters used in Fig. 2 represent moderate values of the quadrupolar coupling constant. This particular site has a large η value leading to modest FAM enhancement. The enhancements are larger for small η values. Further simulations (not shown) indicate that FAM–RIACT–FAM is even more advantageous for sites with higher C_Q. Note that the optimal parameters of the FAM sequences are not the same for the RAPT application at the beginning of the pulse sequence and for the $(+3) \rightarrow (+1)$ coherence transfer process. Lowering the rf amplitude for the first FAM sequence further enhances the signal. This is presumably because the rough equalisation of the populations across the two satellite transitions is relatively undemanding, while too powerful rf fields tend to partially saturate the $|2\rangle \leftrightarrow |3\rangle$ central transition, leading to a loss of the I_z^{23} density operator component. These factors are under further investigation.

Figure 3 shows a compilation of 3QMAS ^{87}Rb NMR data obtained on polycrystalline $RbNO_3$ using a variety of pulse sequences. The first column shows the isotropic projection of the 2D spectrum, showing peaks from the Rb(1), Rb(2), and Rb(3) sites, resolved according to their isotropic chemical and quadrupolar shifts. The central column shows the anisotropic projections, which corresponds to the conventional MAS spectra. The third column shows a slice through the 2D spectrum at the Rb(3) site. Analysis of this second-order quadrupolar lineshape allows determination of the quadrupole interaction parameters.

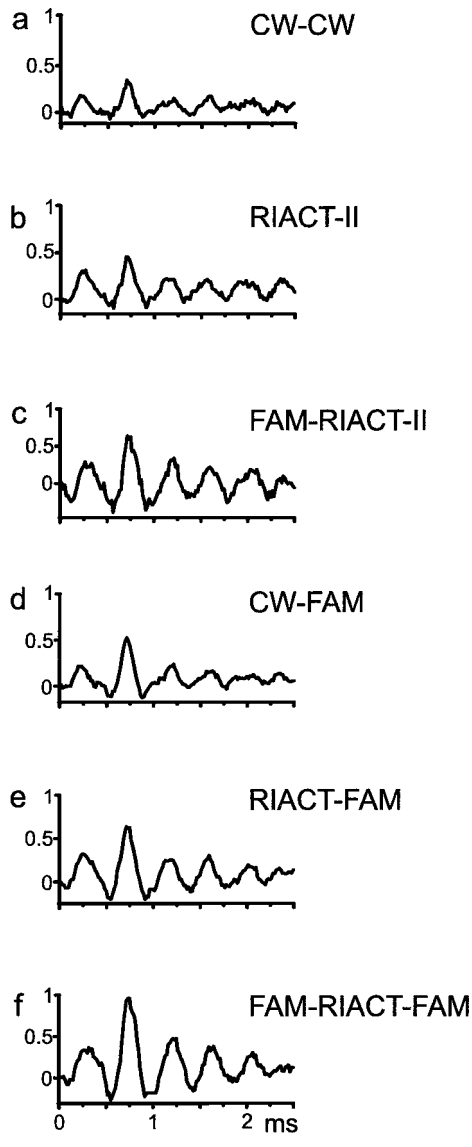

FIG. 2. Numerical simulation of a 3Q echo resulting from various MQMAS pulse schemes for a 3Q evolution time of 900 μs. The simulation parameters correspond to the ^{87}Rb(1) site of $RbNO_3$ (see text) in a field of 4.7 T.

The spectra in 3a, 3b, and 3c were produced with the two-pulse sequence. The isotropic peaks are assigned to the Rb sites in Fig. 3p. Higher intensity was produced with the RIACT-II method, Figs. 3d, 3e, and 3f, but the anisotropic lineshape in Fig. 3f is quite distorted. This is a common observation with RIACT-II (*15*).

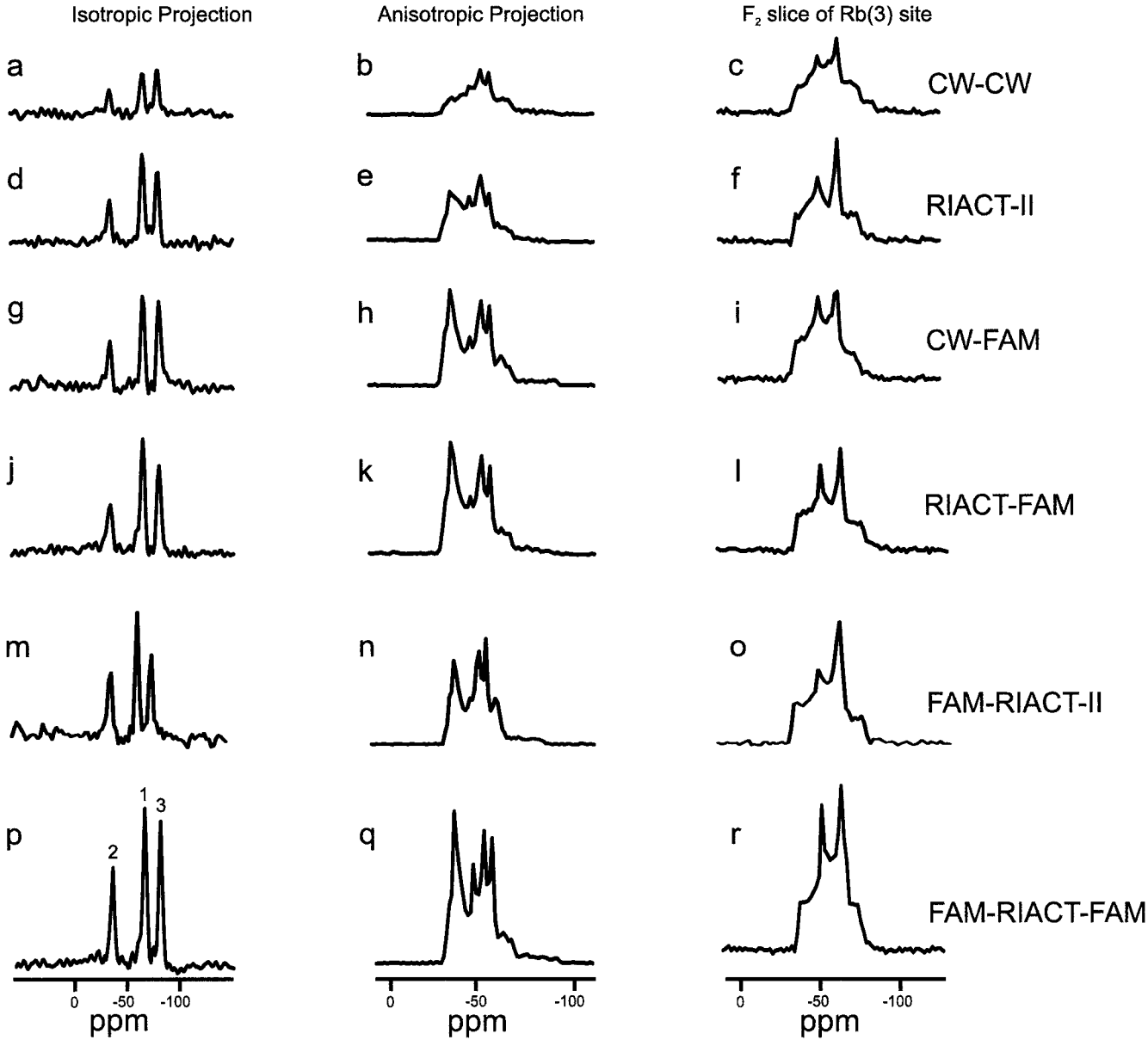

FIG. 3. Isotropic projection of the 3QMAS ^{87}Rb spectra of $RbNO_3$ (column 1), anisotropic projection of the 3QMAS spectra of $RbNO_3$ (column 2), and anisotropic slice corresponding to Rb(2) site (column 3) obtained with MQMAS pulse schemes, CW–CW, RIACT-II, CW–FAM, RIACT–FAM, FAM–RIACT, and FAM–RIACT–FAM.

The spectra in the next two rows were produced by using FAM for the 3Q → 1Q conversion. In Figs. 3g–3i a short CW pulse was used for the 3Q excitation, while in Figs. 3j–3l a RIACT pulse was used. The results are fairly similar.

The fifth row, Figs. 3m–3o, has spectra from the sequence FAM-RIACT-II (also known as RAPT-RIACT-II (*18*)), which has an enhanced signal intensity in comparison with the spectra from the RIACT-II scheme, Figs. 3d–3f. The anisotropic lineshape shows an improvement with respect to that from RIACT-II scheme, but some distortions are still evident.

In the final row, Figs. 3p–3r, results from the new FAM–RIACT–FAM sequence are shown. The signal enhancement is obvious and the anisotropic lineshape shown in Fig. 3r has a clean appearance.

Figure 4 shows a 2D spectrum of the same sample produced by using the FAM–RIACT–FAM sequence. The experimental parameters are the same as before with the number of transients being 384. Also shown are the anisotropic slices from experiments and simulations corresponding to the three Rb sites. For the simulations, using the program SIMPSON (*26*), 4185 quadrupolar orientations were chosen according to the ZCW scheme (*27–29*). The simulations show that the second-order lineshapes are slightly distorted but are still usable for determination of the quadrupolar interaction parameters.

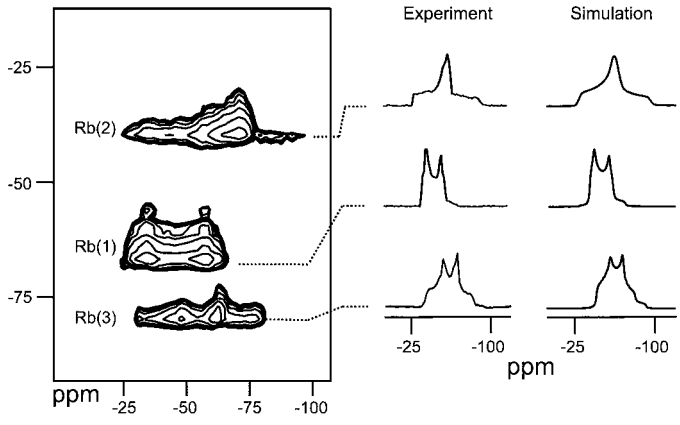

FIG. 4. Two-dimensional 3QMAS ^{87}Rb spectrum of $RbNO_3$ together with anisotropic slices corresponding to the three Rb sites, and corresponding simulations.

In this communication we have shown that the signal strength of the RIACT-FAM scheme (*15*) for spin-$\frac{3}{2}$ can be enhanced by a factor of at least 1.5 by applying a FAM sequence before the rest of the pulse sequence. Experimental results on the ^{87}Rb NMR of $RbNO_3$ indicate that this enhancement is achieved without unacceptable distortions of anisotropic lineshapes.

Further enhancements are conceivable. For example, the RIACT–FAM method exploits the enhanced population difference across the central transition achieved by the first FAM sequence, but does not take advantage of the population difference across the 3Q transition, which is also considerable. Single-pulse excitation, on the other hand, mainly exploits the 3Q population difference to achieve 3Q excitation, but the efficiency is poor. A method which exploits both population differences to achieve 3Q excitation is conceivable, but has not been implemented to the best of our knowledge.

The FAM–RIACT–FAM sequence is probably not optimal for experiments on spin-$\frac{5}{2}$ and higher, since the efficiency of the RIACT transfer is strongly degraded by unwanted level crossings. We have preliminary evidence that good results may be obtained in spin-$\frac{5}{2}$ systems by also replacing the RIACT sequence by FAM leading to a FAM–CW–FAM–FAM sequence. Similar observations have been made by others (*30*). This is under investigation.

ACKNOWLEDGMENTS

This research was supported by Southampton University. Discussions with Shimon Vega and Amir Goldbourt are gratefully acknowledged.

REFERENCES

1. L. Frydman and J. Harwood, Isotropic spectra of half-integer quadrupolar spins from bidimensional MAS NMR, *J. Am. Chem. Soc.* **39,** 5367–5368 (1995).
2. A. Medek, J. S. Harwood, and L. Frydman, Multiple-quantum magic-angle spinning NMR: A new method for the study of quadrupolar nuclei in solids, *J. Am. Chem. Soc.* **117,** 12,779–12,787 (1995).
3. P. J. Dirken, S. C. Kohn, M. E. Smith, and E. R. H. van Eck, Complete resolution of Si–O–Si and Si–O–Al fragments in an aluminosilicate glass by ^{17}O multiple quantum magic angle spinning NMR spectroscopy, *Chem. Phys. Lett.* **266,** 568–574 (1997).
4. S.-J. Hwang, C. Fernandez, J. P. Amoureux, J. C. J.-W. Han, S. W. Martin, and M. Pruski, Structural study of $xNa_2S + (1 - x)B_2S_3$ glasses and polycrystals by MQ-MAS NMR of ^{11}B and ^{23}Na, *J. Am. Chem. Soc.* **120,** 7337–7346 (1998).
5. C. A. Fyfe, H. M. zu Altenschildesche, and J. Skibsted, Characterization of $Na_5P_2O_{10}$ polymorphs by ^{23}Na MAS, ^{23}Na MQMAS and ^{31}P MAS NMR spectroscopy, *Inorg. Chem.* **38,** 84–92 (1999).
6. A. Ferreira, Z. Lin, J. Rocha, C. M. Morais, M. Lopes, and C. Fernandez, *Ab initio* structure determination of a small-pore framework sodium stannosilicate, *Inorg. Chem.* **40,** 3330–3335 (2001).
7. G. Wu, D. Rovnyak, B. Q. Sun, and R. G. Griffin, High-resolution multiple quantum MAS NMR spectroscopy of half-integer quadrupolar nuclei, *Chem. Phys. Lett.* **249,** 210–217 (1996).
8. P. K. Madhu, A. Goldbourt, L. Frydman, and S. Vega, Sensitivity enhancement of the MQMAS NMR experiment by fast amplitude modulation of the pulses, *Chem. Phys. Lett.* **307,** 41–47 (1999).
9. P. K. Madhu, A. Goldbourt, L. Frydman, and S. Vega, Fast radiofrequency amplitude modulation in multiple-quantum magic-angle-spinning nuclear magnetic resonance: Theory and experiments, *J. Chem. Phys.* **112,** 2377–2391 (2000).
10. A. Goldbourt, P. K. Madhu, and S. Vega, Enhanced conversion of triple to single-quantum coherence in the triple-quantum MAS NMR spectroscopy of spin-$\frac{5}{2}$ nuclei, *Chem. Phys. Lett.* **320,** 448–456 (2000).
11. A. P. M. Kentgens and R. Verhagen, Advantages of double frequency sweeps in static, MAS and MQMAS NMR of spin $I = \frac{3}{2}$ nuclei, *Chem. Phys. Lett.* **300,** 435–443 (1999).
12. D. Iuga, H. Schäfer, R. Verhagen, and A. P. M. Kentgens, Population and coherence transfer induced by double frequency sweeps in half-integer quadrupolar spin systems, *J. Magn. Reson.* **147,** 192–209 (2000).
13. H. Schäfer, D. Iuga, R. Verhagen, and A. P. M. Kentgens, Population and coherence transfer in half-integer quadrupolar spin systems induced by simultaneous rapid passages of the satellite transitions: A static and spinning single crystal nuclear magnetic resonance study, *J. Chem. Phys.* **114,** 3073–3091 (2001).
14. G. Wu, D. Rovnyak, and R. G. Griffin, Quantitative multiple quantum magic-angle spinning NMR spectroscopy of quadrupolar nuclei in solids, *J. Am. Chem. Soc.* **118,** 9326–9332 (1996).
15. A. Goldbourt, P. K. Madhu, S. Kababya, and S. Vega, The influence of the radiofrequency excitation and conversion pulses on the lineshapes and intensities of the triple-quantum MAS NMR spectra of $I = \frac{3}{2}$ nuclei, *Solid State Nucl. Magn. Reson.* **18,** 1–16 (2000).
16. The original title of the experiment was SL-FAM (*15*), implying that the first part of the experiment involved spin-locking. This nomenclature (originally used in M. E. Smith and E. R. H. van Eck, *Prog. Nucl. Magn. Reson. Spectrosc.* **34,** 159 (1999)) is misleading since the transverse magnetisation is not spin-locked by the rf field but converted into MQC.
17. Z. Yao, H.-T. Kwak, D. Sakellariou, L. Emsley, and P. J. Grandinetti, Sensitivity enhancement of the central transition NMR signal of quadrupolar nuclei under magic-angle spinning, *Chem. Phys. Lett.* **327,** 85–90 (2000).
18. H.-T. Kwak, S. Prasad, Z. Yao, P. J. Grandinetti, J. R. Sachleben, and L. Emsley, Enhanced sensitivity in RIACT/MQ-MAS experiments using rotor assisted population transfer, *J. Magn. Reson.* **150,** 71–80 (2001).
19. D. Massiot, B. Touzo, D. Trumeau, J. P. Coutures, J. Virlet, P. Florian, and P. J. Grandinetti, Two-dimensional magic-angle spinning isotropic

reconstruction sequences for quadrupolar nuclei, *Solid State Nucl. Magn. Reason.* **6,** 73–83 (1996).

20. S. P. Brown and S. Wimperis, Two-dimensional multiple-quantum MAS NMR of quadrupolar nuclei. Acquisition of the whole echo, *J. Magn. Reson.* **124,** 279–285 (1999).
21. T. Vosegaard, P. Florian, P. J. Grandinetti, and D. Massiot, Pure absorption-mode spectra using a modulated RF mixing period in MQMAS experiments, *J. Magn. Reson.* **143,** 217–222 (2000).
22. M. H. Levitt, "Spin Dynamics. Basics of Nuclear Magnetic Resonance," Wiley, Chichester, UK, 2001.
23. M. H. Levitt, P. K. Madhu, and C. E. Hughes, Cogwheel phase cycling, submitted for publication.
24. C. Fernandez and J. P. Amoureux, Triple-quantum MAS NMR of quadrupolar nuclei, *Solid State Nucl. Magn. Reson.* **5,** 315–321 (1996).
25. S. Vega and Y. J. Naor, Triple-quantum NMR on spin systems with $I = \frac{3}{2}$ in solids, *J. Chem. Phys.* **75,** 75–86 (1981).
26. M. Bak, J. T. Rasmussen, and N. C. Nielsen, SIMPSON: A general simulation program for solid-state NMR spectroscopy, *J. Magn. Reson.* **147,** 296–330 (2000).
27. S. K. Zaremba, Good lattice points, discrepancy, and numerical integration, *Ann. Mat. Pure. Appl.* **293,** 4–73 (1996).
28. H. Conroy, Molecular Schrödinger equation. VIII. A new method for the evaluation of multidimensional integrals, *J. Chem. Phys.* **47,** 5307–5318 (1967).
29. V. B. Cheng, H. H. Suzukawa, Jr., and M. Wolfsberg, Investigations of a nonrandom numerical method for multidimensional integration, *J. Chem. Phys.* **59,** 3992–3999 (1973).
30. A. Goldbourt and S. Vega, Signal enhancement in 5QMAS spectra of spin-$\frac{5}{2}$ quadrupolar nuclei, *J. Magn. Reson.* (in press).